Letter

Forced and natural dynamics of a clamped flexible fiber in wall turbulence

Giulio Foggi Rota, Morie Koseki, Riya Agrawal,* Stefano Olivieri,† and Marco Edoardo Rosti‡

Complex Fluids and Flows Unit, Okinawa Institute of Science and Technology Graduate University, 1919-1 Tancha, Onna-son, Okinawa 904-0495, Japan

(Received 12 May 2023; accepted 21 November 2023; published 12 January 2024)

We characterize the dynamical behavior of a clamped flexible fiber immersed in wall turbulence over a wide range of natural frequencies (f_{nat}) by means of direct numerical simulations. Only two flapping states are possible: one where the fiber oscillates at the characteristic frequency of the largest turbulent eddies (f_{turb}) and another where the natural structural response dominates. The former is obtained in the more flexible cases ($f_{nat} < f_{turb}$), while the latter in the more rigid ones ($f_{nat} > f_{turb}$). We observe that in the turbulence-dominated regime, the fiber always sways at a frequency proportional to the largest scale of the flow, regardless of its structural parameters. The hindrance of the clamp to the wall prevents the synchronization of the fiber with turbulent eddies of comparable size.

DOI: 10.1103/PhysRevFluids.9.L012601

Atmospheric winds and marine currents often interact with the solid surface of the Earth, giving rise to geophysical boundary layers. Those are frequently disturbed by the presence of slender and flexible obstacles, either natural or artificial, which protrude from the ground. The gentle swaying of a tree in the wind or the dangerous oscillations of a pylon are only a couple of demonstrations of the rich dynamical behavior which emerges as a consequence of the complex fluid-structure interaction discussed in this Letter.

When a multitude of slender objects is uniformly distributed over a region that is wide compared to their height (e.g., trees in a forest or seaweed on the seafloor, but also cilia on a membrane), a canopy is attained [1–5]. With some noticeable exceptions in the field of microfluidics [6], the flow above and within a canopy is typically turbulent. The turbulent flow established within and immediately above a canopy differs significantly from a conventional boundary layer since the structure of turbulence is altered [7–12] and the diffusion of passive species (such as suspended sediments, seeds, and pollutants) is enhanced [13–17]. Recently, considerable effort has been spent to investigate the features of the flow and the dynamics of the flexible canopy elements [18–21]; nevertheless, the dynamics of a single constitutive element was not characterized in detail. This study therefore represents a step back from the existing body of works and aims to numerically characterize the behavior of a clamped flexible fiber immersed in wall turbulence for different values of its rigidity, length, and density. We provide solid ground for a thorough understanding of more

*Currently at United College of Engineering and Research, Allahabad 211010, Uttar Pradesh, India.
†Currently at Universidad Carlos III de Madrid, Leganés, 28911 Madrid, Spain.
‡marco.rosti@oist.jp

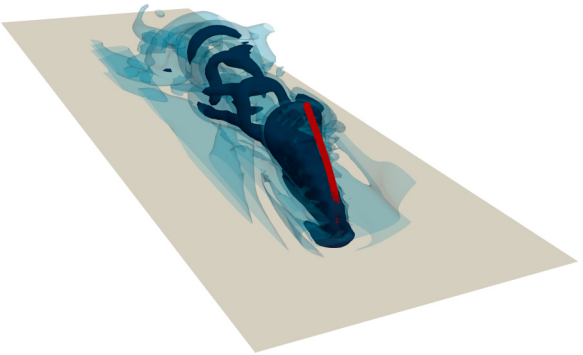

FIG. 1. Flexible fiber clamped in a turbulent wall flow. The fiber is colored in red, while the flow structures behind the fiber are visualized as blue isosurfaces of the vorticity magnitude, $|\omega|$. Light and dark correspond to $|\omega| = 6.5U_b/H$ and $|\omega| = 15.5U_b/H$, respectively.

complex systems composed of several elements, where the relation between their individual and collective dynamics becomes important.

In this Letter, we show how the dynamical response of a flexible fiber immersed in a *wall bounded turbulent flow* (such as the one depicted in Fig. 1) can only vary among two different regimes, depending on its structural properties. Specifically, the fiber is observed to either oscillate at its natural frequency, f_{nat}, or sway at a rate comparable to that of the largest turbulent eddies in the flow, f_{turb}. While the former scenario is attained when $f_{\text{nat}}/f_{\text{turb}} \gg 1$, the latter corresponds to a condition where $f_{\text{nat}}/f_{\text{turb}} \ll 1$ and the flapping frequency of the fiber becomes independent of its structural properties.

To tackle this fluid-structure interaction problem, we numerically solve a modified version of the Euler-Bernoulli equations, which well describe the dynamics of an inextensible elastic fiber, coupled to the Navier-Stokes equations, which fully represent the motion of the incompressible Newtonian fluid in which the isolated fiber is immersed. The setup adopted is that of a conventional turbulent channel flow at a Reynolds number $\text{Re} = U_b 2H/\nu = 5600$, where a fluid of kinematic viscosity ν streams with a mean bulk-averaged velocity U_b along the positive x direction, between two no-slip planes at a distance $2H$ in the y direction. We investigate the behavior of almost rigid fibers as well as flexible ones, spanning different values of the Cauchy number, Ca, defined as the ratio among the force exerted by the fluid and the restoring elastic force opposed by the fiber, $\text{Ca} = (\rho_f d h^3 U_b^2)/(2\gamma)$, where ρ_f is the volumetric density of the fluid, d is the cross-section diameter of the fiber, h is its length, and γ its bending rigidity. In particular, we vary the Cauchy number by varying the length of the fiber, h, or its bending rigidity γ, and the density ratio between fiber and fluid, ρ_s/ρ_f, by varying the fiber density ρ_s. Further details on the values of the relevant parameters employed throughout our simulations and about our numerical setup are provided in the Supplemental Material [22].

The most evident effect of the flow on a clamped fiber is the deflection of its time-averaged position: the fiber reconfigures its shape, bending in the streamwise direction proportionally to the value of Ca, and experiences a reduced drag compared to its typical quadratic scaling with the velocity, especially when the hydrodynamic force is most intense [23–25]. The fiber reconfiguration is shown in Fig. 2, where black lines denote its time-averaged positions for different values of Ca. Instead, the gray regions represent the envelope in which the fiber oscillates. The amplitude of the oscillations increases while moving away from the root and depends on both the structural properties of the fiber (namely, Ca and ρ_s; more details on this can be found in the Supplemental Material [22]) and the turbulent state of the flow at the wall-normal distance where the fiber is located, overall exhibiting a nonmonotonic trend.

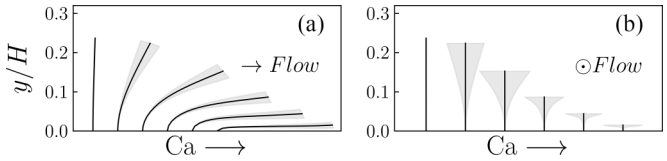

FIG. 2. Time-averaged configuration (black lines) of the fiber that is $0.25H$ long for logarithmically increasing values of Ca in the range $[3.1 \times 10^{-2}, 3.1 \times 10^{3}]$: (a) side and (b) front views. The fiber is deflected by the mean flow according to its rigidity, and hence oscillates about its time-averaged configuration. Gray regions show the root mean square of the displacement from the time-averaged configuration.

To better understand the relation between the motion of the fluid and that of the fiber, we compare the probability density functions (PDFs) [26] of their respective velocities. For the fiber, we consider the velocity of the tip (where the motion is most pronounced) and compute the *Lagrangian* PDF from its time history. For the fluid, instead, we take into account the velocity fluctuations in a channel at the same Re without the fiber and compute the *Eulerian* PDF from the space and time signal measured at a wall-normal position correspondent to that of the deflected tip. On comparing the Eulerian and Lagrangian PDFs, two different behaviors are observed when varying the rigidity of the fiber. At a high value of Ca, the PDFs of the fiber overlap well with those of the flow up to absolute values of the velocity that are twice as big as the root mean square (rms) of the flow velocity fluctuations for both the spanwise [Fig. 3(a)] and wall-normal components. This is indicative of a regime where the fiber, deflected forward by the current, coherently sways with the turbulent fluctuations in the directions not forced by the mean flow and does not exhibit any independent dynamics. The flow also dominates the streamwise dynamics of the fiber, but the inextensibility constraint and the clamp to the wall hinder its motion. After reaching a critical value of Ca (which lays roughly in the middle of our investigated range), all the PDFs of the fiber start widening and drift away from those of the flow [Fig. 3(b)], as the fiber moves independently. Further decreasing Ca always leads to states where the PDFs of the flow and of the fiber do not match.

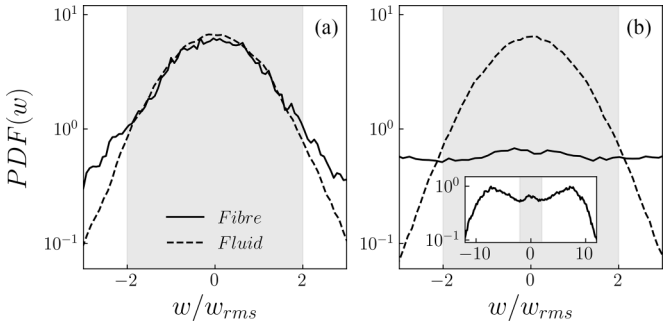

FIG. 3. Different regimes of motion of the fiber, identified with the PDFs of the spanwise velocity component w (i.e., the only one not directly affected by the presence of the mean flow and the inextensibility constraint, or by the confinement of the walls). Solid lines refer to the data taken from the fiber tip velocity, while dashed lines are associated to the flow velocity fluctuations measured at a wall distance corresponding to the mean position of the deflected fiber tip. The rms of w at such position, denoted w_{rms}, is adopted to adimensionalize w itself. (a) A flexible fiber ($\mathrm{Ca} = 3.1 \times 10^2$, $h = 0.25H$, $\rho_s = 1.08\rho_f$) for which the two PDFs overlap, hence suggesting that the fiber is moving with the flow. (b) A more rigid fiber ($\mathrm{Ca} = 3.1$, $h = 0.25H$, $\rho_s = 1.08\rho_f$) for which the two PDFs are radically different, thus hinting at an independent motion of the fiber. On a wider scale (inset), the PDF of the fiber appears bimodal and compatible with nearly sinusoidal oscillations.

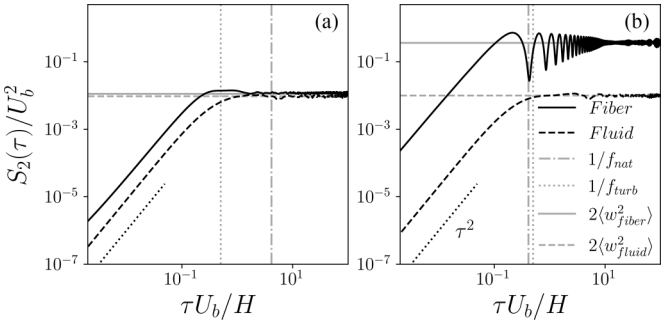

FIG. 4. Second-order structure function of the spanwise velocity component w. Solid black lines refer to the Lagrangian data taken from the fiber tip velocity, while dashed black lines are associated to the Eulerian flow velocity fluctuations measured at a wall distance corresponding to the mean position of the deflected fiber tip. (a) A flexible fiber ($\mathrm{Ca} = 3.1 \times 10^2$, $h = 0.25H$, $\rho_s = 1.08\rho_f$) for which S_2 saturates at $\tau \approx 1/f_{\mathrm{turb}}$, reaching a value $2\langle w^2_{\mathrm{fiber}}\rangle \approx 2\langle w^2_{\mathrm{fluid}}\rangle$, highlighting the passive motion of the fiber in the flow. (b) A more rigid fiber ($\mathrm{Ca} = 3.1$, $h = 0.25H$, $\rho_s = 1.08\rho_f$) for which the natural response is visible and the saturation value does not correspond to that of the fluid, suggesting an independent motion of the fiber.

The existence of two different regimes of motion for the fiber, as well as their main features, can also be appreciated by comparing the second-order Lagrangian temporal structure function of the fiber tip spanwise velocity to the Eulerian one of the fluid, at the mean position of the deflected fiber tip. In Fig. 4, we therefore observe $S_2(\tau) = \langle [w(t+\tau) - w(t)]^2 \rangle$ for the same two fibers considered in Fig. 3. In both cases, for the smallest values of the separation τ, $S_2 \sim \tau^2$ follows directly from the Taylor expansion of S_2 as τ goes to 0: the fluctuating signal w is smooth over those timescales. The signal decorrelates [$\langle w(t+\tau) - w(t)\rangle \approx 0$] for larger values of τ and the behavior of the fiber emerges. In the most flexible case [Fig. 3(a)], the Lagrangian structure function associated to the motion of the fiber saturates at $\tau \approx 1/f_{\mathrm{turb}}$, reaching a value of $2\langle w^2_{\mathrm{fiber}}\rangle \approx 2\langle w^2_{\mathrm{fluid}}\rangle$, suggesting that the motion of the fiber is coupled to that of the fluid. In the most rigid case [Fig. 3(b)], instead, the fiber exhibits its natural response, which is decoupled from the turbulent fluctuations of the flow and characterized by nearly sinusoidal oscillations [as confirmed by the bimodal nature of the fiber PDF on the larger scale reported in the inset of Fig. 3(b)]. The Lagrangian structure function associated to the motion of the fiber has local minima at $\tau \approx 1/f_{\mathrm{nat}}$ and higher harmonics [where $f_{\mathrm{nat}} \approx 3.516/(dh^2)\sqrt{\gamma/(\rho_s \pi^3)}$ is the natural frequency of the fiber], and saturates at a different value from that of the fluid.

Interestingly, our results bear similarities with previous investigations in the field of vortex-induced vibration (VIV) [27]. Despite the significant differences in the setup (our clamped fiber is extremely slender and flexible, while VIV investigations mainly deal with more rigid and intrusive bluff bodies, with usually only one or two degrees of freedom), we identify two regimes of motion: one in which the fiber follows the flow and one in which it independently oscillates at its natural frequency. We are now keen to better investigate and understand the dynamics of the fiber by sampling the motion of its tip for a sufficiently long time span, removing any initial transient and looking at the frequency spectra. After inspecting the Fourier transforms of all the displacement and velocity components, we decide to focus once again on the spanwise velocity: conclusions similar to those drawn in the following could also be reached by observing the other components, while dealing with a more disturbed signal affected by external constraints. Two scenarios are possible, as shown in Fig. 5: When the fiber is flexible and sways with the flow (as previously established from the PDFs), the spectrum exhibits a broad-band peak [Fig. 5(a)], spread over roughly a decade. Instead, when the fiber is more rigid and sways at its natural frequency (as previously established from the second-order structure functions), the peak is narrower and more prominent [Fig. 5(b)]. In this second case, we confirm that the frequency of the peak corresponds to the natural frequency of the fiber.

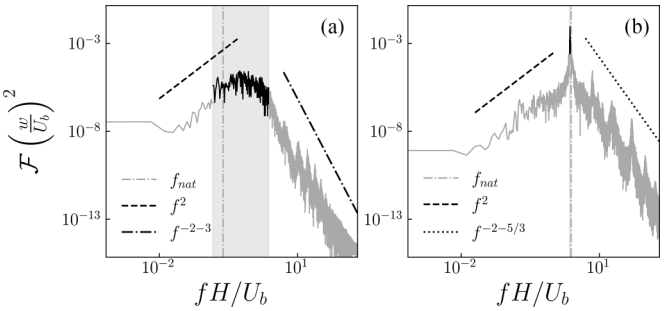

FIG. 5. Spectra of the tip spanwise velocity w for (a) a flexible ($\mathrm{Ca} = 3.1 \times 10^2$, $h = 0.25H$, $\rho_s = 1.08\rho_f$) and (b) a more rigid ($\mathrm{Ca} = 3.1$, $h = 0.25H$, $\rho_s = 1.08\rho_f$) fiber. In the former, the broad-band peak of the signal spans roughly a decade of frequencies, while in the latter, the peak is narrow and more prominent; we emphasize this difference by shading the region among the two frequencies at which the signal achieves a value that is one decade below its maximum, approaching the peak from the left and from the right. By representing the natural frequency of the fiber with a vertical dashed line, we confirm that the more rigid fiber, in (b), is exhibiting its natural response. Both spectra follow a f^2 scaling in the low-frequency region by construction. After the peak, instead, the fiber exhibits a $f^{-2+\xi}$ decay, with $\xi = -3$ for the flexible fiber, characteristic of a smooth regime, and with $\xi = -5/3$ for the more rigid one, typical of fully developed turbulence.

The spectra always follow a f^2 scaling in the low-frequency region by construction, being the transform of a Lagrangian velocity signal, while at high frequencies they decay according to a $f^{-2+\xi}$ law [28,29]. When the fiber is more flexible, it is deflected in the lower part of the viscous wall region ($0.05 \lesssim y/H \lesssim 0.1$) by the mean flow and oscillates under the forcing of a smooth turbulent field, thus hinting towards a $\xi = -3$ decay of the spectrum [30]. This argument is well supported by the high-frequency range of our data in Fig. 5(a). When the fiber is more rigid, instead, it spans the buffer layer and turbulence takes over, thus justifying the recovery of the conventional $\xi = -5/3$ exponent. We therefore point out the interesting counterposition between the dynamics of a more rigid fiber, dominated by its natural response but "reflecting" the turbulent flow in the high-frequency range, and that of a more flexible one, dominated by the flow but forced by the smooth turbulent field to which the fiber is exposed as a consequence of its deflection in the near-wall region. The temporal spectra of the turbulent kinetic energy at the mean position of the deflected fiber tip, representing the forcing to which the fiber is exposed, are reported in the Supplemental Material [22].

The analysis of the single spectrum conducted above proves informative, but not exhaustive: the location of the transition between the two oscillation regimes remains unknown and the physical meaning associated to the frequency of the spectral peak f_{flap} is unclear in the more flexible cases. To tackle these issues, we investigate multiple values of the parameters Ca, h/H, and ρ_s/ρ_f; we therefore extract f_{flap} for each case [31] and compare the outcomes. For the highest values of Ca considered in this study, the fiber is observed to oscillate at $f_{\mathrm{flap}} \approx 0.5U_b/H$ regardless of its structural parameters. We therefore set $f_{\mathrm{turb}} = 0.5U_b/H$ and map every case on a $f_{\mathrm{flap}}/f_{\mathrm{turb}}$ vs $f_{\mathrm{nat}}/f_{\mathrm{turb}}$ diagram in Fig. 6, where f_{nat} is a direct consequence of the choice of the structural parameters and it scales as $f_{\mathrm{nat}}/f_{\mathrm{turb}} \propto \mathrm{Ca}^{-0.5}$ upon fixing h/d and ρ_s/ρ_f. As shown in Fig. 6, the two regimes of motion of the fiber appear as two very distinct branches on the diagram: for $f_{\mathrm{nat}}/f_{\mathrm{turb}} \ll 1$, the data plateaus, confirming our previous observation that $f_{\mathrm{flap}} \cong f_{\mathrm{turb}}$, while for $f_{\mathrm{nat}}/f_{\mathrm{turb}} \gg 1$, the data collapse on a line with unitary slope, highlighting that $f_{\mathrm{flap}} \cong f_{\mathrm{nat}}$. The horizontal branch therefore corresponds to the condition in which the fiber is compliant with the turbulent fluctuations of the flow: independently from the choice of the structural parameters, the dominant spectral component of the tip motion lays at a frequency dictated by turbulence. The apparent absence of any relation among the value of f_{turb} sampled by the fiber and its structural characteristics is a interesting phenomenon, demanding further experimental verification. On the other hand, the structural parameters play a major role along the ascending branch of the diagram,

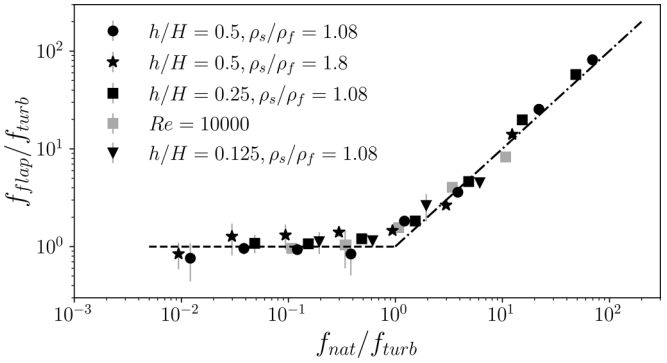

FIG. 6. Values of the spanwise flapping frequency (f_{flap}) as a function of the fiber natural frequency (f_{nat}). All frequencies are scaled with respect to the turbulent frequency measured by the most flexible filaments, $f_{\text{turb}} = 0.5U_b/H$. The error bars represent the variation in the measured value of f_{flap} when halving the time history.

where they set the value of the natural frequency at which the fiber oscillates. The transition between the two regimes occurs at $f_{\text{nat}}/f_{\text{turb}} \approx 1$. Finally, we investigate the physical reasons justifying the value of f_{flap} measured along the horizontal branch of the diagram, when $f_{\text{nat}}/f_{\text{turb}} \ll 1$ and the fiber always oscillates at the same frequency. We observe that the timescale $1/f_{\text{flap}} \approx 2H/U_b$ is comparable to the turnover time of the largest eddies in the flow, which span the whole width of the channel and contain most of the overall turbulent kinetic energy. Simulating an additional turbulent channel flow at $\text{Re} = 10\,000$, we confirm that the flapping frequency of a fiber satisfying $f_{\text{nat}}/f_{\text{turb}} \ll 1$ is proportional to the largest flow scale and not to the turbulent eddies of size comparable to the fiber length. High-Re results are reported as gray squares in Fig. 6.

The existence of two distinct dynamical regimes for the fiber is in qualitative agreement with previous works studying free fibers suspended in homogeneous isotropic turbulence (HIT) [10,32–34], notwithstanding the anisotropic and nonhomogeneous nature of the flow we considered here, thus hinting towards a more general behavior of slender flexible bodies in turbulent flows. Nevertheless, a substantial quantitative difference here is that the fiber is clamped to the wall, which hinders its motion and prevents it from following the flow in a Lagrangian way. Because of this, the flapping state of the fiber nontrivially relates to the largest scale of the flow and not to the turbulent eddies of comparable size, as previously found for the free fibers [10,32–34]. This behavior, contrasting with any previous result, is observed here and is the main outcome of this Letter.

In this study, we have shown that a clamped flexible fiber immersed in a turbulent wall flow can exhibit only two different regimes of motion, depending on how its structural properties (and hence its natural frequency f_{nat}) relate to a characteristic turbulent frequency proportional to the largest scale of the flow, f_{turb}. For $f_{\text{nat}}/f_{\text{turb}} \gg 1$, the fiber oscillates at its natural frequency, while for $f_{\text{nat}}/f_{\text{turb}} \ll 1$, it sways at f_{turb} regardless of its structural parameters. We also notice that the existence of a state where the turbulent fluctuations are passively followed by the fiber, as highlighted by the PDFs in Fig. 3, retains practical relevance since quantities of engineering interest, such as the flow rate or the Reynolds number, can be measured relying on this phenomenon.

This research was supported by the Okinawa Institute of Science and Technology Graduate University (OIST) with subsidy funding from the Cabinet Office, Government of Japan. The authors acknowledge the computer time provided by the Scientific Computing section of the Research Support Division at OIST, and by RIKEN, under the HPCI System Research Project Grant No. hp220402 on the FUGAKU supercomputer. S.O. acknowledges the support from Grants No. FJC2021-047652-I and No. PID2022-142135NA-I00 by MCIN/AEI/10.13039/501100011033 and European Union NextGenerationEU/PRTR. R.A. thanks OIST for the Research Internship program, during which she contributed to this work.

[1] M. R. Raupach and A. S. Thom, Turbulence in and above plant canopies, Annu. Rev. Fluid Mech. **13**, 97 (1981).
[2] J. Finnigan, Turbulence in plant canopies, Annu. Rev. Fluid Mech. **32**, 519 (2000).
[3] H. M. Nepf, Flow and transport in regions with aquatic vegetation, Annu. Rev. Fluid Mech. **44**, 123 (2012).
[4] Y. Brunet, Turbulent flow in plant canopies: Historical perspective and overview, Boundary-Layer Meteorol. **177**, 315 (2020).
[5] E. Loiseau, S. Gsell, A. Nommick, C. Jomard, D. Gras, P. Chanez, U. D'Ortona, L. Kodjabachian, J. Favier, and A. Viallat, Active mucus–cilia hydrodynamic coupling drives self-organization of human bronchial epithelium, Nat. Phys. **16**, 1158 (2020).
[6] W. Wang, Q. Liu, I. Tanasijevic, M. F. Reynolds, A. J. Cortese, M. Z. Miskin, M. C. Cao, D. A. Muller, A. C. Molnar, E. Lauga, P. L. McEuen, and I. Cohen, Cilia metasurfaces for electronically programmable microfluidic manipulation, Nature (London) **605**, 681 (2022).
[7] D. Poggi, A. Porporato, L. Ridolfi, J. D. Albertson, and G. G. Katul, The effect of vegetation density on canopy sub-layer turbulence, Boundary-Layer Meteorol. **111**, 565 (2004).
[8] M. Ghisalberti and H. M. Nepf, The limited growth of vegetated shear layers, Water Resour. Res. **40**, 2003WR002776 (2004).
[9] A. Sharma and R. García-Mayoral, Turbulent flows over dense filament canopies, J. Fluid Mech. **888**, A2 (2020).
[10] S. Olivieri, L. Brandt, M. E. Rosti, and A. Mazzino, Dispersed fibers change the classical energy budget of turbulence via nonlocal transfer, Phys. Rev. Lett. **125**, 114501 (2020).
[11] A. Monti, S. Nicholas, M. Omidyeganeh, A. Pinelli, and M. E. Rosti, On the solidity parameter in canopy flows, J. Fluid Mech. **945**, A17 (2022).
[12] S. Nicholas, M. Omidyeganeh, and A. Pinelli, Numerical investigation of regime transition in canopy flows, Flow, Turbul. Combust. **109**, 1133 (2022).
[13] M. Luhar, J. Rominger, and H. Nepf, Interaction between flow, transport and vegetation spatial structure, Environ. Fluid Mech. **8**, 423 (2008).
[14] M. Mossa, M. Ben Meftah, F. De Serio, and H. M. Nepf, How vegetation in flows modifies the turbulent mixing and spreading of jets, Sci. Rep. **7**, 6587 (2017).
[15] P. A. Makar, R. M. Staebler, A. Akingunola, J. Zhang, C. McLinden, S. K. Kharol, B. Pabla, P. Cheung, and Q. Zheng, The effects of forest canopy shading and turbulence on boundary layer ozone, Nat. Commun. **8**, 15243 (2017).
[16] R. Shnapp, Y. Bohbot-Raviv, A. Liberzon, and E. Fattal, Turbulence-obstacle interactions in the Lagrangian framework: Applications for stochastic modeling in canopy flows, Phys. Rev. Fluids **5**, 094601 (2020).
[17] X. Qin, W. Liang, Z. Liu, M. Liu, C. C. Baskin, J. M. Baskin, Z. Xin, Z. Wang, and Q. Zhou, Plant canopy may promote seed dispersal by wind, Sci. Rep. **12**, 63 (2022).
[18] S. Tschisgale, B. Löhrer, R. Meller, and J. Fröhlich, Large eddy simulation of the fluid–structure interaction in an abstracted aquatic canopy consisting of flexible blades, J. Fluid Mech. **916**, A43 (2021).
[19] J. Wang, G. He, S. Dey, and H. Fang, Fluid–structure interaction in a flexible vegetation canopy in an open channel, J. Fluid Mech. **951**, A41 (2022).
[20] S. He, H. Liu, and L. Shen, Simulation-based study of turbulent aquatic canopy flows with flexible stems, J. Fluid Mech. **947**, A33 (2022).
[21] A. Monti, S. Olivieri, and M. E. Rosti, Collective dynamics of dense hairy surfaces in turbulent flow, Sci. Rep. **13**, 5184 (2023).
[22] See Supplemental Material at http://link.aps.org/supplemental/10.1103/PhysRevFluids.9.L012601 for technical details on the numerical methods and the setup of our simulations, along with additional results, which includes Refs. [21,28,32,35–44].
[23] A. Alben, M. Shelley, and J. Zhang, Drag reduction through self-similar bending of a flexible body, Nature (London) **420**, 479 (2002).
[24] F. Gosselin, E. Langre, and B. A. Machado-Almeida, Drag reduction of flexible plates by reconfiguration, J. Fluid Mech. **650**, 319 (2010).

[25] M. Luhar and H. M. Nepf, Flow-induced reconfiguration of buoyant and flexible aquatic vegetation, Limnol. Oceanogr. **56**, 2003 (2011).
[26] The PDF of a random variable x at a given point (or sample) provides the relative likelihood of x being equal to the sample. It is a well-defined mathematical tool to describe random processes, such as the ones observed in this Letter.
[27] P. W. Bearman, Vortex shedding from oscillating bluff bodies, Annu. Rev. Fluid Mech. **16**, 195 (1984).
[28] Y. Jin, S. Ji, and L. P. Chamorro, Spectral energy cascade of body rotations and oscillations under turbulence, Phys. Rev. E **94**, 063105 (2016).
[29] The theory of Jin *et al.* [28], which is well supported by experimental evidence, provides the general model of the transfer function associated to the velocity oscillations of the structure adopted in this study.
[30] U. Frisch, *Turbulence: The Legacy of A. N. Kolmogorov* (Cambridge University Press, Cambridge, 1995).
[31] All the values of f_{flap} are extracted as the maximum location of the logarithm of the Fourier spectrum of w^2, where only peaks with a prominence of 0.5 computed using a smoothing kernel of 10 points are compared to extract the highestvalues. We have assessed the robustness of the results from the choice of such parameters.
[32] M. E. Rosti, A. A. Banaei, L. Brandt, and A. Mazzino, Flexible fiber reveals the two-point statistical properties of turbulence, Phys. Rev. Lett. **121**, 044501 (2018).
[33] S. Brizzolara, M. E. Rosti, S. Olivieri, L. Brandt, M. Holzner, and A. Mazzino, Fiber tracking velocimetry for two-point statistics of turbulence, Phys. Rev. X **11**, 031060 (2021).
[34] S. Olivieri, A. Mazzino, and M. E. Rosti, On the fully coupled dynamics of flexible fibers dispersed in modulated turbulence, J. Fluid Mech. **946**, A34 (2022).
[35] A. Mazzino and M. E. Rosti, Unraveling the secrets of turbulence in a fluid puff, Phys. Rev. Lett. **127**, 094501 (2021).
[36] J. Kim and P. Moin, Application of a fractional-step method to incompressible Navier-Stokes equations, J. Comput. Phys. **59**, 308 (1985).
[37] F. W. Dorr, The direct solution of the discrete poisson equation on a rectangle, SIAM Rev. **12**, 248 (1970).
[38] Z. Yu, A DLM/FD method for fluid/flexible-body interactions, J. Comput. Phys. **207**, 1 (2005).
[39] A. A. Banaei, M. E. Rosti, and L. Brandt, Numerical study of filament suspensions at finite inertia, J. Fluid Mech. **882**, A5 (2020).
[40] W. X. Huang, S. J. Shin, and H. J. Sung, Simulation of flexible filaments in a uniform flow by the immersed boundary method, J. Comput. Phys. **226**, 2206 (2007).
[41] C. S. Peskin, The immersed boundary method, Acta Numer. **11**, 479 (2002).
[42] S. Yoshihiko, T. Tetsuro, N. Hirotsugu, and K. Tadanori, Experimental study on flow over rigid vegetation simulated by cylinders with equispacing, Transactions of the Japan Society of Civil Engineers **438**, 31 (1991).
[43] J. Jiménez and P. Moin, The minimal flow unit in near-wall turbulence, J. Fluid Mech. **225**, 213 (1991).
[44] J. Kim, P. Moin, and R. Moser, Turbulence statistics in fully developed channel flow at low Reynolds number, J. Fluid Mech. **177**, 133 (1987).